In Situ Characterization of β-Amyloid in Alzheimer's Diseased Tissue by Synchrotron Fourier Transform Infrared Microspectroscopy

Lin-P'ing Choo,*# David L. Wetzel,§ William C. Halliday,¶ Michael Jackson*, Steven M. LeVine,‖ and Henry H. Mantsch*

*Institute for Biodiagnostics, National Research Council Canada, Winnipeg, Manitoba, Canada; #Department of Biochemistry and Molecular Biology, University of Manitoba, Winnipeg, Manitoba, Canada; §Microbeam Molecular Spectroscopy Laboratory, Kansas State University, Manhattan, Kansas, USA; ¶Department of Pathology, Health Sciences Centre, Winnipeg, Manitoba, Canada; and ‖Department of Physiology, University of Kansas Medical Center, Kansas City, Kansas, USA

ABSTRACT We report the first evidence of the structure of β-amyloid protein as it exists in situ within a slice of human Alzheimer's diseased brain tissue. Using a Fourier transform infrared microspectroscopic technique, areas of interest can be selected for spectral measurements with regions of potential contamination masked. In so doing, it is possible to obtain infrared spectra only of β-amyloid and not the surrounding grey matter within which it lies. However, to obtain spectra of high-quality signal-to-noise ratio using a conventional infrared source, we were limited to aperture sizes between 24 μm × 24 μm to 50 μm × 50 μm. Markedly improved high-quality spectra were acquired with infrared radiation provided by a synchrotron light source (National Synchrotron Light Source, Brookhaven National Laboratories), using aperture sizes as small as 12 μm × 12 μm. This allowed spectroscopic mapping of brain tissue regions containing amyloid. We observe that in situ proteins of grey matter exist predominantly in an α-helical and/or unordered conformation, whereas within amyloid deposits a β-sheet structure predominates. The hydrogen bonding strength of the β-structure found in situ is different from that reported in the literature for isolated/chemically synthesized β-amyloid peptides.

INTRODUCTION

Alzheimer's disease (AD) is the most common form of dementia, with the clinical symptoms of memory loss, disorientation in person, time and place, and cognitive decline (McKhann et al., 1984; Katzman and Jackson, 1991). Autopsy investigation of the AD brain reveals gross cortical atrophy, narrow gyri, widened sulci, and enlarged ventricles (Khachaturian, 1985; Mirra et al., 1993). At the cellular level, microscopic analysis reveals neuronal loss, synaptic loss, reactive gliosis, amyloid angiopathy, and the formation of neurofibrillary tangles and neuritic plaques in the cortical regions of the brain (Khachaturian, 1985; Mirra et al., 1993). Neuritic plaques (NPs) exist extracellularly in the cortex of the AD brain and contain insoluble amyloid (accummulated aggregated proteins and peptides) deposits surrounded by abnormal neuronal processes (Mirra et al., 1993). It has been suggested that amyloid deposition is important (although not necessarily the only key event) in the pathogenesis of AD (Selkoe, 1994; Sisodia and Price, 1995).

The amyloid of AD brains is composed primarily of amyloid β-peptide (Aβ, also known as βA4), which is a 4-kDa, 39–43-amino acid peptide derived from the larger amyloid β-precursor protein (AβPP) (Maury, 1995). AβPP is expressed throughout the central nervous system, although its role(s) is not well defined. Its ubiquitous presence and the high degree of sequence conservation between species suggest that AβPP plays an important role(s) in the biology of neural cells. Abnormal cleavage of AβPP results in the accumulation of Aβ in the AD brain. Aβ's role in any part of the development of AD clinical phenotypes, or in the generation of neuritic plaques, neurofibrillary tangles, and neuronal death is not yet fully understood. However, in vitro studies have demonstrated Aβ to be neurotoxic (Yankner et al., 1989), and Aβ has been shown to nucleate rapidly into amyloid fibrils, possibly serving as a seed for the aggregation and subsequent deposition of amyloid extracellularly (Jarrett et al., 1993). In addition, Aβ may interact with surrounding proteins such as apolipoprotein E to enhance the formation of amyloid fibrils (Strittmatter et al., 1993).

In view of the potential role of Aβ in AD pathology, there has been much focus on examining the structure of Aβ to elucidate the structural properties that may dictate the seeding event of fibril formation (Jarrett et al., 1993). An understanding of the structure-function relationship of this peptide as it relates to AD pathology may provide insights for developing new methods of early diagnosis and treatment. Circular dichroism (CD), NMR spectroscopy, x-ray diffraction, and Fourier transform infrared (FTIR) spectroscopy have been used extensively to study the structure of Aβ (Barrow and Zagorski, 1991; Fraser et al., 1991, 1992, 1993, 1994; Zagorski and Barrow, 1992; Fabian et al., 1993, 1994; Inouye et al., 1993; Ötvös et al., 1993). In all of these studies, either fragments or the whole Aβ peptide has been isolated or chemically synthesized for investigation under a variety of conditions (extremes of pH, in organic solvents, etc.). Depending on the solution conditions, synthetic Aβ peptides can adopt mixtures of β-sheet, α-helix, and unordered structures. Studies on the 1–42-amino acid β-amyloid

Received for publication 9 April 1996 and in final form 16 July 1996.

Address reprint requests to Dr. Henry H. Mantsch, Institute for Biodiagnostics, National Research Council of Canada, 435 Ellice Ave., Winnipeg, MB R3B 1Y6 Canada. Tel.: 204-984-4624; Fax: 204-984-5472; E-mail: mantsch@ibd.nrc.ca.

0006-3495/96/10/1672/08 $2.00

peptide in aqueous solution have found that the peptide adopts a β-aggregated conformation involving intermolecular hydrogen bonding (Barrow and Zagorski, 1991; Fabian et al., 1993). It has also been demonstrated that the hydrophobic carboxyl terminal sequence, Aβ 29–42, adopts an oligomeric β-strand structure in solution regardless of differences in solvent, pH, and temperature (Barrow and Zagorski, 1991). On the other hand, the structure of the N-terminal domain and residues 1–28 varies with the solution conditions; at pH 1–4 and above pH 7, a monomeric α-helical structure predominates, whereas between pH 4 and pH 7 the fragment adopts a β-strand conformation (Barrow and Zagorski, 1991; Fraser et al., 1991; Zagorski and Barrow, 1992). However, as many of these studies are performed on synthetic Aβ and/or fragments of Aβ in solution, often under nonphysiological conditions (extremes of pH and temperature, trifluoroethanol solution to solubilize the protein aggregate), one is uncertain whether the structures reported truly reflect the conformation of Aβ as it exists in the AD brain, particularly given the apparent sensitivity of the peptide to its environment.

In this study we present results of the first in situ spectroscopic study of amyloid in the Alzheimer's diseased brain, performed on intact slices of AD brain tissue using Fourier transform infrared (FTIR) microspectroscopy involving IR radiation provided by a synchrotron light source. This synchrotron-based approach to IR microscopy allowed very high quality spectra to be obtained at high spatial resolution (12 μm × 12 μm), thus permitting the detection and analysis of individual neuritic plaques within tissue.

MATERIALS AND METHODS

Human autopsy tissue

Histopathologically confirmed control and Alzheimer's diseased human autopsy brain tissues were obtained from the Health Sciences Centre (Winnipeg, MB) and the National Neurological Research Specimen Bank (Los Angeles, CA). Age-matched control tissue displayed no abnormalities with respect to cortical atrophy, little presence of neuritic plaques, and the absence of neurofibrillary tangles upon microscopic examination. There was no clinical history of cognitive decline or central nervous system disease and no sign of head trauma. AD tissue was derived from individuals with established long-term dementia who had been in chronic care. AD brains exhibited severe cortical atrophy of the cerebral hemisphere with narrowed gyri, widened sulci, and ventricular enlargement. Histopathological analysis revealed innumerable neuritic plaques, neurofibrillary tangles, and cerebral amyloid angiopathy. The magnitude of these pathological changes led to the diagnosis of definite AD according to the accepted Khachaturian criteria (1985) and revised criteria by Mirra et al. (1993).

Infrared spectroscopy

Conventional infrared microspectroscopy

Tissue samples (1 cm^3) were excised from formalin (10% v/v formaldehyde-buffered solution) fixed brains and flash frozen in liquid nitrogen. Previous studies in this laboratory have demonstrated that formalin absorptions do not interfere with infrared measurements on thin sections of brain tissue (manuscript in preparation). From the frozen sample, thin slices of brain tissue (8 μm) were obtained using a cryostat. These slices were thaw-mounted on BaF_2 optical windows (13 mm diameter; Wilmad Glass Co., Buena, NJ) and allowed to air dry. For cryotoming purposes, small amounts of O.C.T. (Miles, Elkhart, IN) were used to anchor the frozen tissue (examination of tissue spectra revealed no contaminating IR absorptions from O.C.T.). Tissue sections were viewed with light microscope objectives to identify areas of interest, and infrared spectra were then recorded with a Digilab (Bio-Rad Lab., Cambridge, MA) FTS-60 FTIR microspectrometer containing a conventional thermal infrared light source and a small-element (0.25 mm^2) MCT detector. At each location, the acquisition of spectra in the region 800-4000 cm^{-1} involved collecting 512 interferograms over a 3-min time period. Fourier transformation of the co-added interferograms yielded spectra with a nominal resolution of 4 cm^{-1}. A spectrum of an area of the BaF_2 window containing no tissue was recorded as the background spectrum. Infrared spectra were recorded using aperture sizes of 12 μm × 12 μm, 24 μm × 24 μm, and 50 μm × 50 μm.

Synchrotron infrared microspectroscopy

Tissue specimens were prepared as described above; spectra were acquired using an IRμs FTIR microspectrometer (Spectra-Tech, Shelton, CT) equipped with a small-element (0.25 mm^2) MCT detector and interfaced to a synchrotron light source (National Synchrotron Light Source, Brookhaven National Laboratories, Upton, NY). Again, a spectrum of the BaF_2 window containing no tissue was used as the background. Two mapping experiments were performed on separate tissue sections. In the first, a rectangular region 109 μm × 66 μm was mapped with an aperture size of 12 μm × 12 μm, with 13-μm steps in the horizontal direction and 14-μm steps in the vertical direction. For each 12 μm × 12 μm region, 512 interferograms were acquired over a 3-min time period, signal averaged, and Fourier transformed to generate a spectrum with a nominal resolution of 4 cm^{-1}. For the second map, a rectangular region 299 μm × 208 μm was mapped with 27-μm steps in the horizontal direction and 30-μm steps in the vertical direction. The aperture size was increased to 24 μm × 24 μm to reduce data acquisition time for this large region. With this larger aperture size, 128 interferograms were collected over a 2-min time period, signal averaged, and Fourier transformed to generate spectra with a resolution of 4 cm^{-1}. All spectra were baseline corrected and Fourier smoothed using the IRμs software. From the spectra acquired in the mapping experiments, the integrated area under the amide I band was calculated for each spectrum and plotted as a function of position to produce a three-dimensional surface contour plot. In addition, the corresponding peak frequency of the amide I band was determined from the inflection point of the first derivative spectrum and plotted as a function of position to yield a two-dimensional contour plot.

Histology

The tissue sections from control and diseased brains used to acquire spectra were stained with Congo red, a dye that specifically stains amyloid deposits pink-red. Stained tissues were then examined by light microscopy to confirm the presence and locations of amyloid deposition.

RESULTS AND DISCUSSION

Previous studies from our laboratory have examined control, multiple sclerosis, and Alzheimer's disease tissues using conventional FTIR transmission methods (Choo et al., 1993, 1995). In these studies, we observed that it was not difficult to differentiate between grey matter and white matter, based on differences in spectral features arising from lipids (phospholipids and galactolipids) in white matter. On the other hand, it was more difficult to distinguish control grey matter from AD grey matter; only subtle differences in

the amide I band were observed. However, these differences were inconsistent, making it difficult to reach a firm conclusion. This inconsistency was most likely due to the varying density of amyloid deposits between patients and within tissue sampled from different regions of the same brain. Furthermore, these microscopic plaques may account for only a small proportion of the tissue sample, in which case the characteristic spectroscopic features of the plaque would be masked by absorptions from the surrounding grey matter. In addition, with this approach it is difficult to determine the exact nature of the sample because the morphology of the tissue is destroyed after pressing between windows, making analysis by a neuropathologist impossible.

Conventional infrared microspectroscopy

To improve the chances of observing spectroscopic features characteristic of amyloid in neuritic plaques in situ, infrared microspectroscopy was employed. The FTIR microscope consists of a beam condenser, which focuses the IR radiation onto a small area, thereby allowing investigation of small samples with high optical throughput. With this technique, undesirable tissue areas can be masked and specific areas of interest in the tissue can be investigated. In addition, the use of a movable stage allows tissue to be mapped spectroscopically. This technique has been used previously to examine normal mouse brain tissue in situ (Wetzel and LeVine, 1993). In addition, Hill et al. have employed the infrared microsampling technique to study aluminum silicate deposition in the synapse between nerve cells in AD tissue (Hill et al., 1989).

Spectra recorded from the same location with an infrared microscope attached to a conventional FTIR spectrometer, using 12 μm $\times$ 12 μm, 24 μm $\times$ 24 μm, and 50 μm $\times$ 50 μm aperture sizes, are shown in Fig. 1. The signal-to-noise ratio of the spectrum acquired with a 12 μm $\times$ 12 μm aperture is extremely poor, indicating that only a very small amount of IR light from the source is passing through the aperture and the tissue to reach the detector. However, if the aperture is opened to 24 μm $\times$ 24 μm, there is a marked improvement in the quality of the spectra, although noise still persists, making spectral analysis less reliable. At apertures of 50 μm $\times$ 50 μm, the spectra are of sufficient quality for spectroscopic analysis to be performed. With larger aperture sizes, the number of photons reaching the detector is increased, thereby improving the spectral quality. Simultaneously, however, the sampling area is increased and tissue that may not be of interest, such as the grey matter surrounding neuritic plaques, will be included in the measurement. To improve the spectral quality (i.e., to allow more photons to reach the detector) without increasing the aperture size, the intensity of the infrared source must be increased somehow. This may be accomplished by increasing the voltage supplied to conventional sources (resistively heated ceramic globars). However, this will also result in the generation of significant amounts of heat, which may damage the tissue. Therefore, using an infrared microspectrometer equipped with a conventional infrared thermal emission source, the spatial resolution is limited to between 24 μm $\times$ 24 μm and 50 μm $\times$ 50 μm.

Synchrotron infrared microspectroscopy

To improve spatial resolution without compromising the signal-to-noise ratio, we recorded spectra using an FTIR microspectrometer attached to a synchrotron light source. The intrinsic brilliance of a synchrotron light source is 100-1000 times greater than a traditional thermal emission source (Reffner et al., 1995). Furthermore, the source is highly collimated (thus improving spatial resolution) and nonthermal, thereby eliminating the risk of tissue damage from excess heat production. In Fig. 2 we present the spectra of control and Alzheimer's disease tissue recorded with aperture sizes of 12 μm $\times$ 12 μm and 24 μm $\times$ 24 μm. The differences between white and grey matter are as

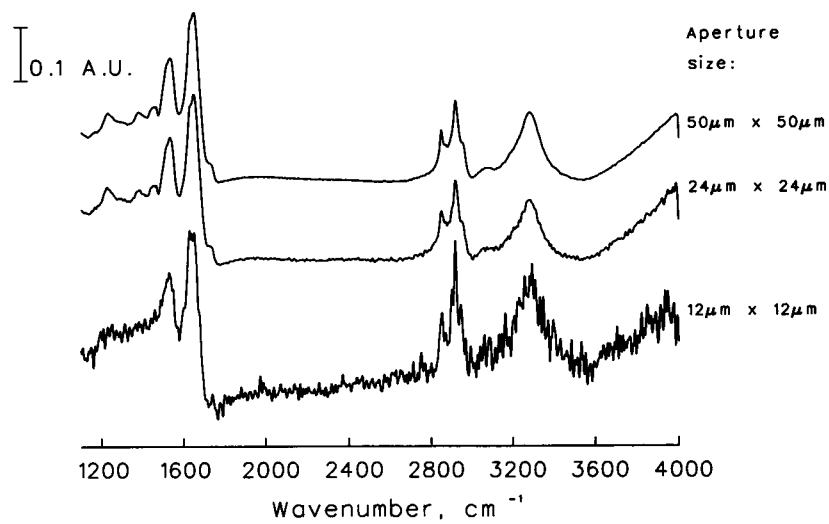

FIGURE 1 Representative IR spectra of a 8-μm-thick slice of AD grey matter recorded at various aperture sizes with a FTIR microspectrometer equipped with a conventional thermal light source.

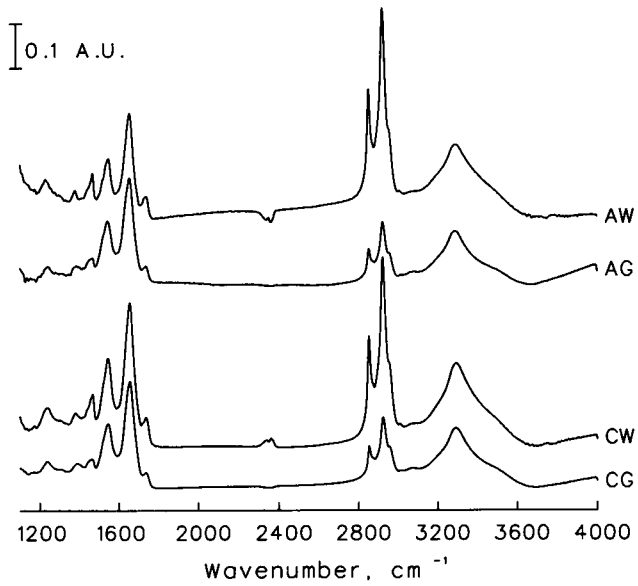

FIGURE 2 Representative IR spectra of 8-μm-thick slices of control grey (CG), control white (CG), Alzheimer's diseased grey (AG), and Alzheimer's diseased white (AW) matter recorded with an FTIR microspectrometer with IR radiation from a synchrotron light source.

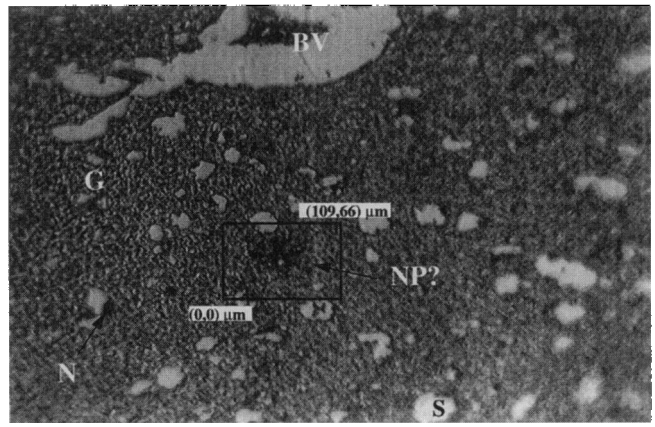

FIGURE 3 Photomicrograph (320× magnification) of a 8-μm-thick slice of AD human grey (G) matter. The tissue contains a suspected neuritic plaque (NP?), part of a blood vessel (BV), cortical neurons (N), and artifactual spaces (S). The region mapped spectroscopically is indicated by the marked rectangle, with coordinates in micrometers.

observed in previous studies. As expected, the spectra have a superior signal-to-noise ratio compared to spectra obtained with a conventional light source (compare with Fig. 1). However, spectra recorded at 12 μm × 12 μm show some deterioration below 1200 cm^{-1}, as the instrument's performance begins to be limited by diffraction properties. As the wavelength of radiation passing through begins to approach the aperture size (1000 cm^{-1} = 10 μm), the radiation is scattered radially upon passing the aperture, resulting in fewer photons reaching the detector and increasing the noise level at low wavenumbers.

Spectroscopic mapping of AD tissue

Having determined that it is possible to obtain high-quality spectra of 12 μm × 12 μm or 24 μm × 24 μm regions of tissue using synchrotron-derived IR radiation, we proceeded to spectroscopically map AD tissue sections at this spatial resolution. The region of tissue outlined in Fig. 3 was chosen for mapping because of the presence of a dense amorphous deposit that was suspected to be a neuritic plaque (labeled NP?) within the grey matter (G). Other morphological features identified in the photomicrograph (magnified 320×) include part of a cerebral blood vessel (BV) and cortical neurons (N) that shrank upon freezing/drying, leaving artefactual spaces (S) or small tears within the specimen (it should be stressed that these artefacts affect only the physical integrity, and not the chemical composition of the sample). From the rectangular region outlined, spectra were obtained with an aperture size of 12 μm × 12 μm, beginning at (0,0) μm and progressing in steps of 13 μm in the horizontal direction (eight spectra acquired). The stage was then moved 14 μm in the y-direction, and a further eight spectra were acquired. This process was continued until the (109,66) μm position was reached. As we are primarily interested in studying the structure of amyloid within neuritic plaques in situ, we specifically examined the infrared spectra in the region between 1500 and 1700 cm^{-1} containing strong bands arising from the amide linkage between amino acid residues. These absorptions, particularly the strong amide I band between 1600 and 1700 cm^{-1} (carbonyl stretching vibration of the amide group), are sensitive to protein secondary structure (Jackson and Mantsch, 1993, 1995). Fig. 4 *A* illustrates the three-dimensional surface contour plot of the integrated intensity of the area under the amide I band for each spectrum corresponding to the region mapped. The values of the x and y axes are the positions along the rectangular region in the photomicrograph, with the z axis representing the integrated band area. The low-intensity areas are represented by red, orange, and yellow, whereas the high-intensity areas are represented by green and blue. The integrated amide I intensity is fairly constant in the regions surrounding the deposit. However, there is a dramatic increase in the intensity of the amide I in the region of the deposit, with a maximum intensity occurring at the center of the feature, [(55,40) μm], indicating a substantial increase in protein concentration at this position.

To further investigate the nature of this protein deposit, a two-dimensional contour plot of the amide I peak frequency as a function of the area mapped is shown in Fig. 4 *B*. Again, the x and y axes correspond to the mapping coordinates, whereas the contour lines and colors represent the peak frequencies; red, orange and yellow represent high frequencies, and blue and green, low frequencies. In the regions surrounding the deposit, the amide I peak frequency is 1652–1654 cm^{-1}, indicative of proteins predominantly in an α-helical and/or unordered structure (Jackson and Mantsch, 1995). However, at the center of the deposit, the

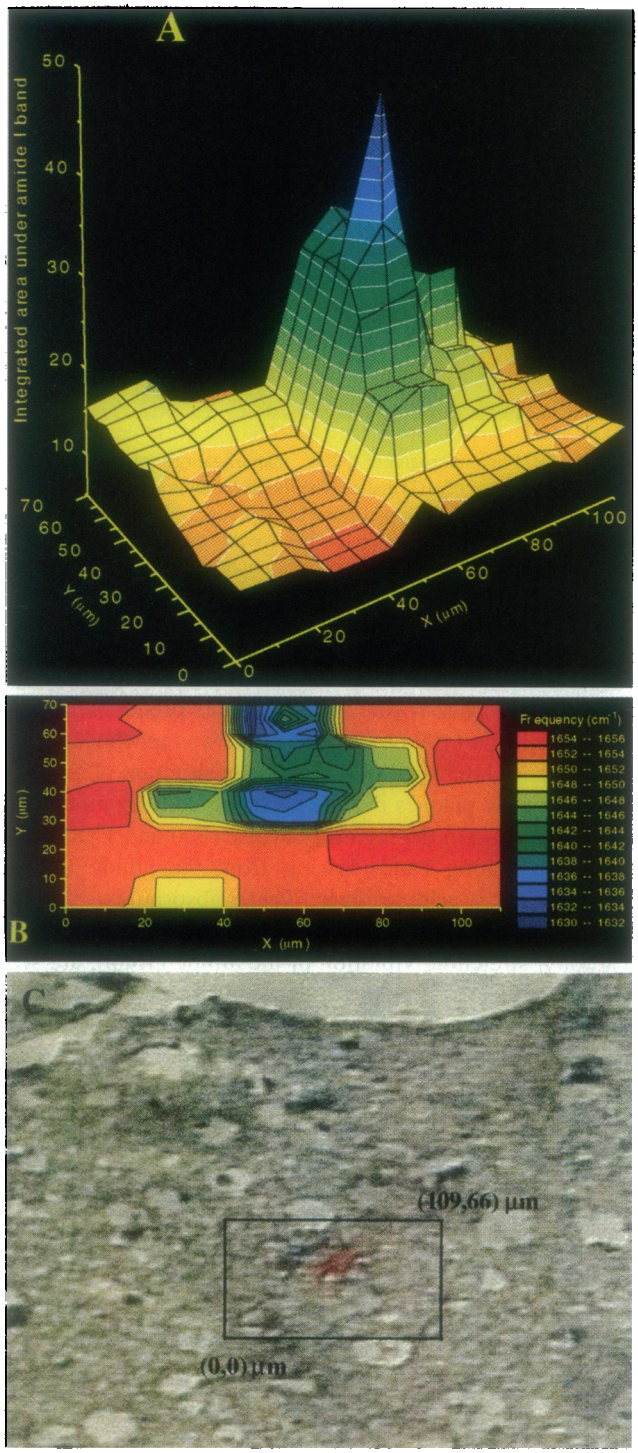

FIGURE 4 (*A*) Three-dimensional surface map of the integrated area under the amide I band corresponding to the rectangular region marked in Fig. 3. (*B*) Two-dimensional contour map of the amide I peak frequency of the region mapped. (*C*) Enlarged photomicrograph of the tissue of interest after staining with Congo red for amyloid (reddish-pink).

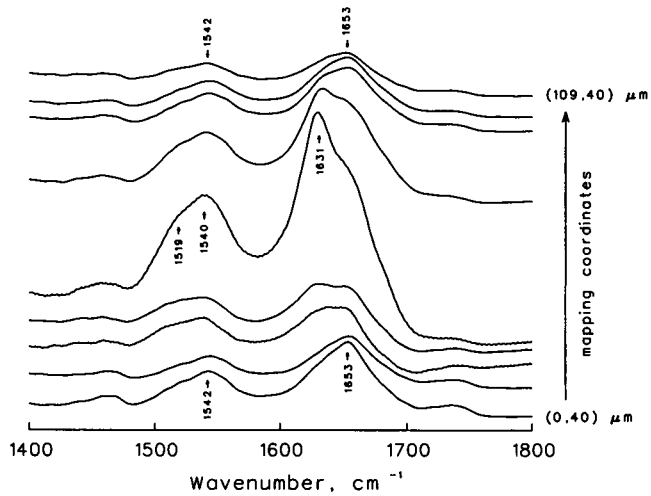

FIGURE 5 Series of IR spectra, plotted in the amide region, extracted from a horizontal strip (0,40) μm to (104,40) μm of the region mapped in Fig. 3.

frequency is shifted to 1632–1634 cm^{-1}, indicating the presence of proteins with a substantially different (β-sheet) conformation. This trend is illustrated more clearly in Fig. 5, which illustrates the amide I region from the series of spectra extracted from a horizontal strip (at about 40 μm in the *y*-position), corresponding to a cross-sectional slice of the map. With increasing mapping coordinates in the horizontal direction, there is a gradual decrease in intensity of the 1653 cm^{-1} absorption with a concomitant increase in the intensity of the 1631 cm^{-1} band. At a position corresponding to the center of the deposit, the 1631 cm^{-1} band is the most prominent absorption. This trend is reversed, moving away from the center to the right edge of the map, corresponding to the surrounding grey matter. Similar trends are observed for the amide II band, which decreases in frequency from 1542 cm^{-1} to 1540 cm^{-1} at the center of the deposit. Our mapping experiment therefore demonstrates that the amorphous deposit in Fig. 3 is predominantly proteinaceous (exhibiting a very intense amide I absorption) and exists in a β-sheet conformation (amide I and II absorption at 1632 and 1540 cm^{-1}, respectively). These results strongly suggest that this feature is the amyloid core of a mature neuritic plaque, a suggestion that was confirmed when the tissue was stained with Congo red, a dye that specifically stains amyloid reddish-pink (magnified region shown in Fig. 4 *C*).

The finding of an amide I maximum at 1632 cm^{-1}, characteristic of β-sheet structures, conflicts with previous IR studies of synthetic amyloid, which demonstrated amide I maxima at significantly lower frequencies (1620–1628 cm^{-1}), indicative of aggregated peptide (Fraser et al., 1991, 1992, 1994; Ötvös et al., 1993; Fabian et al., 1993, 1994). This discrepancy may be the result of the presence of other proteins (e.g., the nonfibrillary amyloid-associated proteins α-1-antichymotrypsin, apolipoprotein E, heparan sulfate proteoglycan, laminin, and ubiquitin) in the neuritic plaque (Maury, 1995). In studies of isolated amyloid, upon aggregation, the peptide can form very strong intermolecular hydrogen bonds because of close alignment of polypeptide chains, resulting in a low amide I frequency. However, in

situ, close alignment of amyloid peptide chains may be prevented by the presence of the other proteins found in the plaque, resulting in the formation of weaker hydrogen bonds and the observation of an amide I at a higher frequency. This indicates that the surrounding proteins play crucial roles in the overall structure of β-amyloid aggregates in vivo and may therefore potentially influence any neurotoxic properties of the amyloid deposit. Future structural studies of β-amyloid and those aimed at examining the effect of potential therapeutics in inhibiting β-amyloid aggregation should therefore carefully consider the presence of surrounding proteins, which we suggest affect the overall structure of the β-amyloid peptide in situ.

The tissue mapped in the previous section contained a relatively large plaque that was fairly easy to identify without staining. However, it is generally more difficult to visually identify areas of amyloid deposition. Fig. 6 is a photomicrograph (magnified 200×) of another region of AD cortical grey matter containing shrunken neuronal cells (N), freezing artifact spaces (S), as well as a cerebral blood vessel (BV) complete with the vascular wall (W) and erythrocytes (E) found within its lumenal space, but no visible neuritic plaques. To determine whether IR spectroscopy could detect the small plaques expected in such tissue, the region indicated by the 299 μm by 208 μm rectangle was mapped. The surface three-dimensional map of the integrated amide I band is shown in Fig. 7 *A*. Across the map, the area of the amide I band is more variable than the previous specimen. There is a region of low intensity indicated by red and orange at around (50,200) μm. Comparing it with the photomicrograph (Fig. 6), this corresponds to the large artifactual space in the tissue (S). There are two major areas of increased intensity, in the upper left-hand and upper right-hand regions of the map, indicated by dark green and blue. This elevated integrated amide I area indicates an increased protein concentration, possibly due to amyloid deposition.

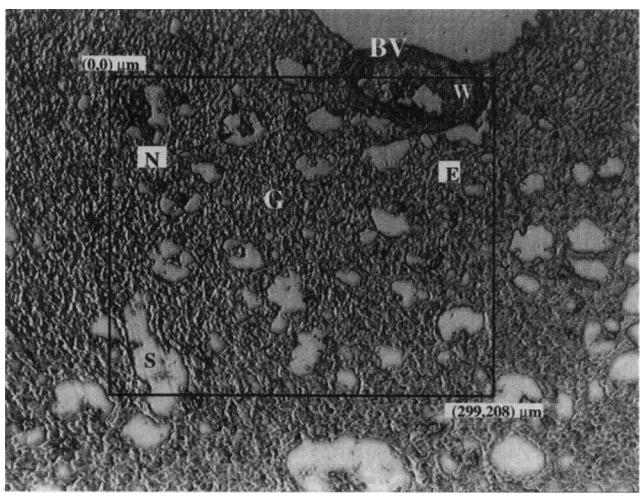

FIGURE 6 Photomicrograph (200× magnification) of an 8-μm-thick slice of human AD grey (G) matter containing several shrunken neuronal cells (N), freezing artifact spaces (S), and a cerebral blood vessel (BV) complete with the vascular wall (W) and erythrocytes (E). The region mapped spectroscopically is indicated by the marked rectangle with coordinates in micrometers.

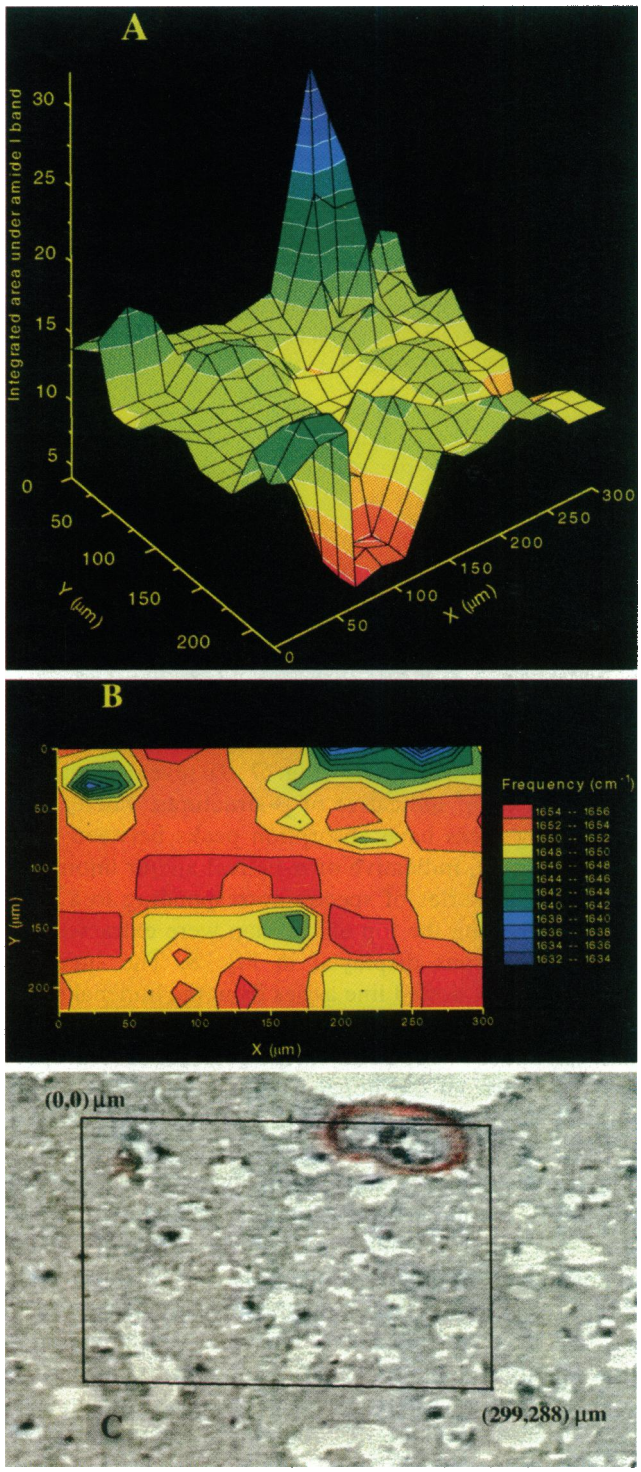

FIGURE 7 (*A*) Three-dimensional surface map of the integrated area under the amide I band corresponding to the rectangular region marked out in Fig. 6. (*B*) Two-dimensional contour map of the amide I peak frequency of the region mapped. (*C*) Enlarged photomicrograph of the tissue of interest after staining with Congo red for amyloid (reddish-pink).

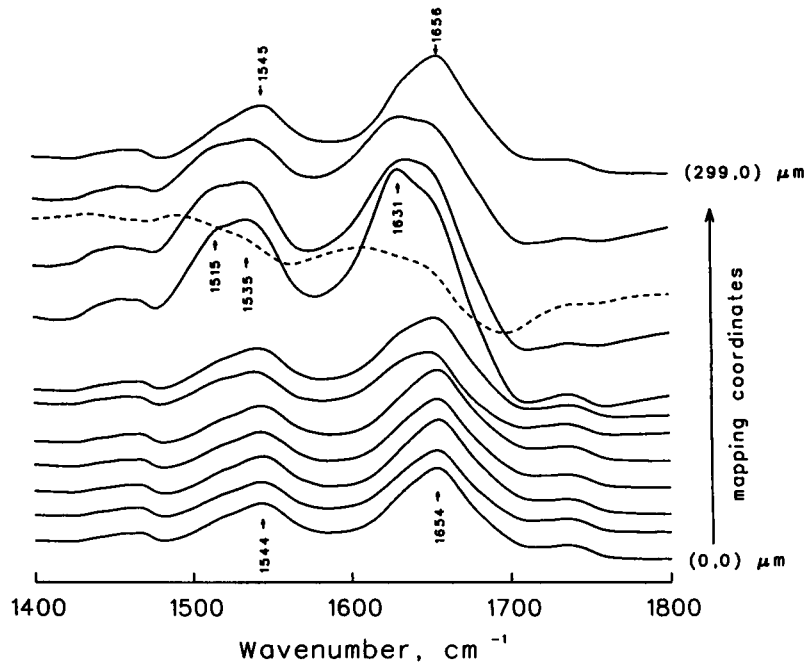

FIGURE 8 Series of spectra plotted in the amide region extracted from a horizontal region (0, 0) μm to (299,0) μm of the region mapped in Fig. 6.

Examination of the amide I peak frequencies corresponding to these regions (Fig. 7 *B*) reveals bands at 1632–1634 cm^{-1} indicative of β-structures, whereas the surrounding areas have absorption peaks between 1650 and 1656 cm^{-1}, indicative of α-helical and/or unordered structure. The series of spectra corresponding to a horizontal strip along the top of the map were extracted and the amide regions displayed in Fig. 8. The spectrum indicated by the dotted line arises from the lumenal space of the blood vessel. In most spectra, the amide I band is observed at 1654–1656 cm^{-1}. However, for several spectra extracted from the upper right corner of the region mapped, [(0,200) μm to (0,270) μm], the major band is at 1631 cm^{-1}, with a minor shoulder at 1654 cm^{-1}. Similar low-frequency shifts were observed in the amide II band. Based upon the findings described for the previous specimen, the observed intense 1631 cm^{-1} band suggests that amyloid deposits exist in the upper right and left corners of the area mapped. It may be suggested that the 1631 cm^{-1} band in spectra of the upper right corner is attributable to specific components intrinsic to the blood vessel wall. However, previous infrared microimaging studies of arteries report protein amide I frequencies between 1650 and 1653 cm^{-1} from various sections of the arterial wall (Kodali et al., 1991). Therefore, our observations are not due simply to strong components of the blood vessel wall, but are most likely due to amyloid deposition. After staining with Congo red dye, pink coloration is observed in the upper left region and around the walls of the blood vessel (Fig. 7 *C*). These areas of histologically demonstrated amyloid deposition correspond exactly to the green/blue colored areas in Fig. 7 *B*, confirming our spectroscopic observations. Thus we have successfully demonstrated the deposition of amyloid within grey matter (neuritic plaques) and within a cerebral blood vessel (amyloid angiopathy, the presence of amyloid within the walls of blood vessels, which can lead to complications such as cerebral hemorrhage and infarction; Maury, 1995).

In summary, using FTIR synchrotron microspectroscopy, we have successfully measured spectra of human control and Alzheimer's diseased brain tissue with a spatial resolution as high as 12 μm × 12 μm, dimensions that come close to the size of single cells. To the best of our knowledge, this is the first study in which regions of grey matter containing extracellular amyloid deposit in situ and amyloid angiopathy were identified spectroscopically. These observations were confirmed by standard histological techniques (staining with Congo red dye).

L.-P. Choo gratefully acknowledges studentship support from the Manitoba Health Research Council. We thank the National Synchrotron Light Source, Brookhaven National Laboratories (Upton, NY), for the beam time to conduct our experiments, as well as Dr. Gwyn Williams, Dr. Lawrence Carr, and Dr. Douglas VanCampen for their invaluable help while at Brookhaven. We also acknowledge tissue sources from the Health Sciences Centre (Winnipeg, MB), as well as the National Neurological Research Specimen Bank (Los Angeles, CA). This paper was issued as NRCC publication no. 34775.

REFERENCES

Barrow, C. J., and M. G. Zagorski. 1991. Solution structures of β peptide and its constituent fragments: relation to amyloid deposition. *Science.* 253:179–182.

Choo, L.-P., M. Jackson, W. C. Halliday, and H. H. Mantsch. 1993. Infrared spectroscopic characterisation of multiple sclerosis plaques in the human central nervous system. *Biochim. Biophys. Acta.* 1182: 333–337.

Choo, L.-P., J. R. Mansfield, N. Pizzi, R. L. Somorjai, M. Jackson, W. C. Halliday, and H. H. Mantsch. 1995. Infrared spectra of human central nervous system tissue: diagnosis of Alzheimer's disease by multivariate analyses. *Biospectroscopy.* 1:141–148.

Fabian, H., L.-P. Choo, G. I. Szendrei, M. Jackson, W. C. Halliday, L. Ötvös, and H. H. Mantsch. 1993. Infrared spectroscopic characterization of Alzheimer plaques. *Appl. Spectrosc.* 47:1513–1518.

Fabian, H., G. I. Szendrei, H. H. Mantsch, B. D. Greenberg, and L. L. Ötvös. 1994. Synthetic post-translationally modified human Aβ peptide exhibits a markedly increased tendency to form β-pleated sheets in vitro. *Eur. J. Biochem.* 221:959–964.

Fraser, P. E., L. Lévesque, and D. R. McLachlan. 1993. Biochemistry of Alzheimer disease amyloid plaques. *Clin. Biochem.* 26:339–349.

Fraser, P. E., D. R. McLachlan, W. K. Surewicz, C. A. Mizzen, A. D. Snow, J. T. Nguyen, and D. A. Kirschner. 1994. Conformation and fibrillogenesis of Alzheimer Aβ peptides with selected substitution of charged residues. *J. Mol. Biol.* 244:64–73.

Fraser, P. E., J. T. Nguyen, H. Inouye, W. K. Surewicz, D. J. Selkoe, M. B. Podlisny, and D. A. Kirschner. 1992. Fibril formation by primate, rodent, and Dutch-hemmoragic analogues of Alzheimer amyloid β-protein. *Biochemistry.* 31:10716–10723.

Fraser, P. E., J. T. Nguyen, W. K. Surewicz, and D. A. Kirschner. 1991. pH-dependent structural transitions of Alzheimer amyloid peptides. *Biophys. J.* 60:1190–1201.

Hill, S. L., K. Krishnan, and J. R. Powell. 1989. Infrared microtransmission and microreflectance of biological systems. *Proc. SPIE.* 1145:400–402.

Inouye, H., P. E. Fraser, and D. A. Kirschner. 1993. Structure of β-crystallite assemblies formed by Alzheimer β-amyloid protein analogues: analysis by x-ray diffraction. *Biophys. J.* 64:502–519.

Jackson, M., and H. H. Mantsch. 1993. Biomembrane structure from FT-IR spectroscopy. *Spectrochim. Acta Rev.* 15:53–69.

Jackson, M., and H. H. Mantsch. 1995. The use and misuse of FTIR spectroscopy in the determination of protein structure. *Crit. Rev. Biochem. Mol. Biol.* 30:95–120.

Jarrett, J. T., E. P. Berger, and P. T. Lansbury. 1993. The carboxy terminus of the β amyloid protein is critical for the seeding of amyloid formation: implications for the pathogenesis of Alzheimer's disease. *Biochemistry.* 32:4693–4697.

Katzman, R., and J. E. Jackson. 1991. Alzheimer disease: basic and clinical advances. *J. Am. Ger. Soc.* 39:516–525.

Khachaturian, Z. S. 1985. Diagnosis of Alzheimer's disease. *Arch. Neurol.* 42:1097–1105.

Kodali, D. R., D. M. Small, J. Powell, and K. Krishnan. 1991. Infrared micro-imaging of atherosclerotic arteries. *Appl. Spectrosc.* 45: 1310–1317.

Maury, C. P. J. 1995. Biology of disease. Molecular pathogenesis of β-amyloidosis in Alzheimer's disease and other cerebral amyloidoses. *Lab. Invest.* 72:4–16.

McKhann, G., D. Drachman, M. Folstein, R. Katzman, D. Price, and E. M. Stadlan. 1984. Clinical diagnosis of Alzheimer's disease: report of the NINCDS-ADRDA work group under the auspices of department of health and human services task force on Alzheimer's disease. *Neurology.* 34:939–944.

Mirra, S. S., M. N. Hart, and R. D. Terry. 1993. Making the diagnosis of Alzheimer's disease. *Arch. Pathol. Lab. Med.* 117:132–144.

Ötvös, L., G. I. Szendrei, V. M.-Y. Lee, and H. H. Mantsch. 1993. Human and rodent Alzheimer β-amyloid peptides acquire distinct conformations in membrane-mimicking solvents. *Eur. J. Biochem.* 211:249–257.

Reffner, J. A., P. A. Martoglio, and G. P. Williams. 1995. Fourier transform infrared microscopical analysis with synchrotron radiation: the microscope optics and system performance. *Rev. Sci. Instrum.* 66: 1298–1302.

Selkoe, D. J. 1994. Alzheimer's disease: a central role for amyloid. *J. Neuropathol. Exp. Neurol.* 53:438–447.

Sisodia, S. S., and D. L. Price. 1995. Role of β-amyloid protein in Alzheimer's disease. *FASEB J.* 9:366–370.

Strittmatter, W. J., A. M. Saunders, D. Schmechel, M. Pericak-Vance, J. Enghild, G. S. Salvesen, and A. D. Roses. 1993. Apolipoprotein E: high avidity binding to β-amyloid and increased frequency of type 4 allele in late-onset familial Alzheimer disease. *Proc. Natl. Acad. Sci. USA.* 90: 1977–1981.

Wetzel, D. L., and S. M. LeVine. 1993. In situ FT-IR microspectroscopy and mapping of normal brain tissue. *Spectroscopy.* 7:40–45.

Yankner, B. A., L. R. Dawes, S. Fisher, L. Villa-Komaroff, M. L. Oster-Granite, and R. L. Neve. 1989. Neurotoxicity of a fragment of the amyloid precursor associated with Alzheimer's disease. *Science.* 245: 417–420.

Zagorski, M. G., and C. J. Barrow. 1992. NMR studies of amyloid β-peptides: proton assignments, secondary structure, and mechanism of an α-helix β-sheet conversion for a homologous, 28-residue, N-terminal fragment. *Biochemistry.* 31:5621–5631.